Journal of Molecular Graphics and Modelling 38 (2012) 50–59

Contents lists available at SciVerse ScienceDirect

Journal of Molecular Graphics and Modelling

journal homepage: www.elsevier.com/locate/JMGM

Homology modeling, docking and molecular dynamics of the *Leishmania mexicana* arginase: A description of the catalytic site useful for drug design☆

Carlos A. Méndez-Cuesta, Oscar Méndez-Lucio, Rafael Castillo*

Facultad de Química, Departamento de Farmacia, Universidad Nacional Autónoma de México, Mexico, DF 04510, Mexico

ARTICLE INFO

Article history:
Accepted 2 August 2012
Available online 10 August 2012

Keywords:
Homology
Arginase
Leishmania mexicana
Docking
Molecular dynamic

ABSTRACT

The crystallographic structure of the *Leishmania mexicana* arginase, an attractive target for the design of leishmanicidal agents, is still unknown. For this reason, we report a computer-assisted homology study conducted to build its three-dimensional structure based on the known sequence of amino acids of this enzyme. In this study, the amino acid sequence in the arginase of the parasite was compared with the sequence of the amino acids in the crystallographic structure of rat and human liver arginases. The best similarity was found with the rat liver arginase. The catalytic site of the three-dimensional arginase structure built for *L. mexicana* has important structural differences as compared with that of the human liver arginase with regard to reasonable design selective compounds against *L. mexicana*. With this information, a docking study was conducted to find the inhibitors of this enzyme. 1439 molecules were docked and 18 were selective to the *L. mexicana* arginase. Moreover, molecular dynamics were carried out to study the stability of the homologue protein (including manganeses) and the ligand–enzyme complex. The results indicated that the manganese remains inside the protein throughout the simulation. Besides, hydrogen bonds interactions between the ligand and the arginase were analyzed. These results provide important information for the design of new inhibitors.

1. Introduction

Protozoa parasites are responsible for most of the common and devastating diseases affecting humans and domestic animals, threatening the lives of one third of the world population [1]. Among these parasites, *Leishmania* spp, a hemo protozoan, stands out as the etiological cause of leishmaniasis, a disease that currently lacks safe and efficient drugs for its treatment. This parasitic disease causes a high number of deaths in many tropical and subtropical regions, thus becoming a major health problem in developing countries [2,3]. In Latin America, the infection exists virtually in all countries [4]. In Mexico, it has affected people since the pre-Hispanic era [5]. Today, the causal agent, now known as *Leishmania mexicana*, is widely distributed throughout the country [6–9].

The disease-causing organisms are several species and subspecies of *Leishmania* (including *L. donovani*, *L. infantum*, *L. mexicana* and *L. amazonensis*) which are transmitted to humans by the bite of a female sandfly of the subfamily *Phlebotominae* [3,10,11]. *Leishmania* spp has a digenetic life cycle that includes a flagellated and mobile form called a promastigote, which resides in the sandfly, and a motionless and intracellular form called an amastigote, which multiplies within macrophages of the infected individual, thus avoiding the immune system [12].

The treatment of leishmaniasis is difficult, a fact that is associated with a high degree of morbidity. Generally, the first-choice drugs are Pentavalent antimonials (SbV), such as sodium Stibogluconate (Pentostam) and Meglumine antimoniate (Glucantime). However, these types of drugs present difficulties because of their toxicity and the pain caused by 20 injections of oily material. Moreover, there are several reports of treatment failure, which results from parasite resistance to antimony. Areas such as Bihar in India reported resistance in 70% of the patients treated for visceral leishmaniasis [13–15]. Treatment with Pentamidine isethionate and Amphotericin B (including liposomal formulation) may represent a clinical cure despite their toxicity. In fact, Amphotericin B is the first-choice drug for visceral leishmaniasis in regions where high resistance to treatment with sodium Stibogluconate has been presented. The use of Paromomycin has also been explored, since it has demonstrated efficacy that is similar to Amphotericin B and it is cheaper. A new drug, Miltefosine, has recently been introduced in the market with the great advantage of being able to be administered orally. Nevertheless, the teratogenic effects presented by Miltefosine represent a main disadvantage for further development [13–15].

Since the available treatments for leishmaniasis involve many problems, the discovery of new leishmanicidal agents is of the utmost importance. For this reason, researchers are now looking

☆ Taken in part from the PhD dissertation of Carlos A. Méndez-Cuesta.

* Corresponding author. Tel.: +52 5556225287; fax: +52 55562255329.
E-mail address: rafaelc@unam.mx (R. Castillo).

1093-3263/$ – see front matter © 2012 Elsevier Inc. All rights reserved.
http://dx.doi.org/10.1016/j.jmgm.2012.08.003

for novel biochemical targets in order to develop new drugs. In the last two decades experimental approaches such as gene-cloning, protein crystallography and transfer RNA have been introduced to validate and define new targets for drugs against this parasite [16–18]. One approach in our research was to use *Leishmania* arginase (L-arginine amidinohydrolase, GenBank ID: AAR06176.1) as a possible drug target. This enzyme is a binuclear manganese metalloenzyme that catalyses the hydrolysis of L-arginine to L-ornithine, urea and ATP [19]. It is also involved in the process of invasion and evasion of the host immune system by reducing the concentration of L-arginine, a molecule that activates the nitric oxide synthase (NOS). As a consequence, the generation of nitric oxide in the macrophages is also reduced and the immune response of the host against the parasite is delayed. This evidence brings to light the biological importance of the *Leishmania* arginase and suggests that it could be used as a relevant drug target against this parasite [20].

To date, there have been no reports on the three-dimensional structure of the *L. mexicana* arginase. However, previous homology modeling studies conducted in the structural determination of the *L. amazonensis* arginase can be used as a guideline for generating three-dimensional models of the *L. mexicana* arginase [19]. Herein, we report the homology modeling and molecular dynamics of the *L. mexicana* arginase, including a deep study of its catalytic site. Furthermore, the differences between this enzyme and the human arginase were analyzed in order to determine the potential for the design of new selective inhibitors. Finally, the *L. mexicana* arginase model and the human arginase crystallographic structure were used for a virtual screening, including 1439 compounds.

2. Materials and methods

2.1. Homology modeling

The amino acid sequence of the *L. mexicana* arginase (GenBank: AAR06176.1) was obtained from the NCBI database [21]. The search for sequential homologues to this amino acid sequence was carried out by using crystal structure reported on this database and various search methods online: GenSilico (https://genesilico.pl/meta2) [22]; PDB/BLAST (http://blast.ncbi.nlm.nih.gov/Blast.cgi) [23]; Bioinfobank (http://meta.bioinfo.pl) [24]. The sequence alignments were performed with the Clustal-W program server (http://www.ebi.ac.uk/Tools/clustalw2/index.html) [25]. The models were built with three different programs: Bioinfobank (http://meta.bioinfo.pl) [24], 3D-Jigsaw (http://bmm.cancerresearchuk.org/~3djigsaw/) [26,27] and MODELLER 9v1 [28,29]. MODELLER is a general program that implements comparative protein structure modeling by satisfying spatial restraints in terms of probable density functions. The resulting models were evaluated by using PROCHECK to assess the quality of the stereochemistry of the protein structure [30]. Moreover, WHATCHECK [31] and PROMOTIF [31,32], which automatically identify, classify and analyze a number of changes in secondary structure, were used for the verification of protein structures. All these methods of assessment were employed on the SWISS-MODEL server [33].

All the models were submitted to an energy-minimization using Sybyl8.0 in order to remove bad contacts derived from the homology modeling [34,35]. All the calculations were carried out in the Amber 4 force field, assigning Gasteiger–Hückel charges at 300 K with a dielectric constant of 4 and with a maximum of 100,000 iterations.

2.2. Virtual screening

A virtual screening against the homology model of the *L. mexicana* arginase and the *Homo sapiens* arginase (PDB ID: 2aeb) was carried out with AutoDock 4.2 [41]. Compounds from zinc (http://zinc.docking.org/), a database that contains more than 21 million molecules that satisfy Lipinski's rules and with a benzimidazole nucleus were selected for this study. A total of 1386 compounds were obtained from zinc and were complemented with a set of 53 benzimidazole derivatives with antiprotozoa activity previously reported by our laboratory [37–40]. The structure of all these compounds was optimized with the Amber 4 force field as implemented in Sybyl8.0. Finally, torsional roots and branches were identified, and Gasteiger–Marsilli atomic charges were assigned for the 1439 compounds using MGLTools 1.5.4 [41].

Before the docking calculations, all water molecules, ligands and the two Mn^{2+} were removed from each protein (*L. mexicana* and human arginases). Moreover, MGLTools 1.5.4 [41] was used to merge all non-polar hydrogens and to assign Gasteiger charges for each atom of the macromolecule. Three-dimensional grids of size 126 Å × 126 Å × 126 Å with 0.375 Å spacing centered at the center of the protein were calculated for each of the following atom types: H, HD, C, A, N, NA, OA, F, P, S, SA, Cl, Br, and I. Electrostatic and desolvation maps were also calculated.

Molecular docking calculations were performed with AutoDock 4.2, using the Lamarckian genetic algorithm (LGA) for ligand conformational searching. The docking of each molecule consisted of a total of 25 runs that were carried out with an initial population of 150 individuals, a maximum of 25 million energy evaluations, a maximum of 270,000 generations, a mutation rate of 0.02, and a crossover rate of 0.8. The resulting conformations for each molecule were clustered using as a threshold a root-mean-square deviation (RMSD) less than 3.0 Å.

The molecules that bind selectively to the active site of the *L. mexicana* arginase were re-docked with grids of size 60 Å × 60 Å × 60 Å centered in the catalytic site of this enzyme. It is important to mention that all possible binding modes were considered throughout all the calculations. For this purpose, flexibility was allowed for all rotable bonds of the ligand, while the protein was used as a rigid structure.

2.3. Molecular dynamics

The molecular dynamics of the *L. mexicana* arginase with and without a ligand were performed using GROMACS 4.0.5 software. The initial structures of these two simulations were the results of homology modeling and the ligand–enzyme complex with the lowest binding energy. The ligand parameters were calculated with a PRODRG [42] server in the framework of the GROMOS force field, while C6 = 5.751 C12 = 4.517 were employed for the Mn^{2+}. The enzyme and the complex were solvated with water in a periodic cubic box that comprises the enzyme and 0.5 nm of water on all sides. Apart from the two Mn^{2+}, two Na^{+} atoms were added randomly in order to neutralize the charge of the system. All the simulations were carried out at 1 bar and 300 K.

First, an energy minimization of the system, containing around 3179 atoms, was carried out employing the GROMOS96 43a1 force field, a single point charge water model and a time step of 0.002 ps. Electrostatic forces were calculated with the PME implementation of the Ewald summation method, and the Lennard–Jones interactions were calculated within a cut-off radius of 0.9 nm. After energy minimization, the system was equilibrated by 20 ps of MD with position restraints on the enzyme, thus enabling the solvent molecules to relax. Finally, a 3 ns MD was performed in order to

Table 1
Comparison among the several search methods using the GenSilico program.

Search methods	Templates	Score	Identity (%)
PDB/Blast	1d3v	1e−128	40
	2aeb	1e−128	43
	1pq3	1e−122	38
	2cev	1e−113	37
Blastp	2aeb	2e−62	44
	1d3v	3e−59	41
	1pq3	7e−55	39
	2cev	2e−53	38
	2ef5	1e−41	38
Hhsearch	2aeb	100	41
	1pq3	100	38
	2cev	100	37
pcons5	2aeb	7.3565	43
	1pq3	7.2131	38
	1d3v	7.1987	40
	2aeb	7.1471	41
	1pq3	7.1009	38
	2cev	6.8098	37
	2cev	6.7062	37
jmbrank	2aeb	nc	41
	1d3v	nc	41
	1pq3	nc	38
	2cev	nc	37
consens3d	1pq3	184.19	38
	2aeb	184.19	41
	1pq3	183.67	38
	1d3v	183.14	40
	2aeb	182.95	43
	2cev	181.10	37
	2cev	180.14	37

nc: the jmbrank program does not calculate score

assess the stability of the arginase model and the ligand–enzyme complex.

3. Results and discussion

3.1. Homology modeling

Several three-dimensional structures with homologous sequences to the *L. mexicana* arginase were found with three different search methods (GenSilico, PDB/BLAST and Bioinfobank), which are listed in Table 1. Interestingly, two structures with a high percentage of similarity were found in the three search methods (above 40%), which is adequate enough to build a reliable model. These two were the crystal structure of the enzyme arginase of *H. sapiens* (PDB ID: 2aeb [43]) and *Rattus norvergicus* (PDB ID: 1d3v [44]), which share a similarity of 44% and 41% similarity to *L. mexicana*, respectively.

H. sapiens (PDB ID: 1wva [43], 2pho [45], 2aeb [43] and 1pq3 [46]) and *R. norvergicus* sequences (PDB ID: 1d3v [44]) were obtained from the NCBI database [23] and aligned by means of the program Clustal-W (Fig. 1). At the primary structure level, the alignment of the amino acid sequences of the arginase of *L. mexicana* and the human arginase (liver and macrophage) show a high degree of similarity, especially in the catalytic site, as can clearly be observed in Fig. 1. Alignment accuracy is the most crucial step to ensure the quality of the homology model, the multiple sequence alignment having always been a preferred approach for this purpose. However, some differences can be seen: while the human enzyme has a no charged Gly235, *L. mexicana* has a polar uncharged Thr246. This difference could be useful for the design of selective inhibitors against this enzyme.

Different 3D models of the *L. mexicana* arginase were built using as a template each of the five different crystal structures reported for the human and the rat arginase [44–46]. For this purpose, Bioinfobank, MODELLER 9v1 and Jigsaw programs to generate a total of 10 models were used. Each model was minimized using the Sybyl8.0 program with the conditions previously described (Section 2). The stereochemistry of each model was assessed using Ramachandran plots generated with the program PROCHECK [30] (data shown in Table 2). The best results were obtained with the program MODELLER 9v1, which employed the rat liver arginase (1d3v) as a template. The Ramachandran plot for this model indicates that 83.7% of the residues were located in the most favored zones, 15.6% in allowed regions, 0.7% in generously allowed regions and 0.0% in disallowed regions. Based on the Ramachandran plots, the structure of the generated model has a reliability of 99.3%. It is important to mention that the model obtained using the Bioinfobank program and the human arginase (1pq3) as a template had a reliability of 99.6%; nonetheless, the structure generated for this enzyme had 78.3% of the residues located in the most favored zones, which is lower than that obtained from the rat liver arginase. Although information regarding the crystal structure of the human arginase is available (PDB), its active site and its mechanism of action are still unknown.

Table 2
Evaluation of the models obtained by 3D-Jigsaw, Bioinfobank and MODELLER programs. The reference crystallized structures from *Rattus norvergicus* (1d3v) and the *Homo sapiens* arginase (1wva, 2pho, 2aeb and 1pq3) were used as templates.

Program	Model	Template	Evaluation (%)
3D-Jigsaw	3D-Jigsaw-1d3v	1d3v	76.0, 21.7, 1.9, 0.4
3D-Jigsaw	3D-Jigsaw-2aeb	2aeb	71.2, 25.4, 2.7, 0.8
3D-Jigsaw	3D-Jigsaw-2pho	2pho	71.4, 26.3, 0.4, 1.9
Bioinfobank	Bioinfobank-1d3v	1d3v	78.8, 20.0, 0.8, 0.4
Bioinfobank	Bioinfobank-1pq3	1pq3	78.3, 21.3, 0.0, 0.4
Bioinfobank	Bioinfobank-2aeb	2aeb	76.3, 23.3, 0.4, 0.0
Modeller	Modeller-1d3v	1d3v	83.7, 15.6, 0.7, 0.0
Modeller	Modeller-1pq3	1pq3	77.3, 20.2, 1.4, 1.1
Modeller	Modeller-1wva	1wva	77.3, 21.6, 0.7, 0.4
Modeller	Modeller-2aeb	2aeb	73.8, 23.8, 1.8, 0.7

In addition, since the scores found in this study for the rat liver arginase model are within the accepted values, the PROCHECK program showed a global Z-score value of −0.57 obtained from the Ramachandran plot. A Z-score value greater than −2.0 is commonly associated with a high-quality model. The QMEAN [47] score was −0.96, a value slightly lower than the limit of two standard deviations (Fig. 2), but still acceptable for a large protein structure. This score is composed of a linear combination of 6 terms, where the pseudo-energy of the contributing terms is given with respect to the scores obtained for high-resolution experimental structures of similar size solved by X-ray crystallography. The distribution of the types of residues, both within and outside of the protein, is normal, with an inside/outside RMS Z-score value of 1.097. WHATIF Z-score, obtained by assessing the 3D structure through a series of measurements of structures crystallized by X-ray and NMR, was −7.9. To be acceptable, this value must be below −6. Compared with other models, Modeller-1d3v was the most acceptable of all. The reliability of this model makes it apt for molecular docking virtual screening to find new specific inhibitors (*vide infra*).

The amino acids that coordinate Mn^{2+} and the ones that bind arginine in the active site [36] are localized in the same region in the *L. mexicana* arginase model and in the 3D structure of the rat liver arginase (PDB ID: 1d3v). Fig. 3 shows His139, Asp243 and Asp245, which coordinate with one Mn^{2+}; His114, Asp137 and Asp141, which coordinate another Mn^{2+}; and His154 and Glu288, which are directly involved in the arginine binding [48]. These amino acids are conserved in all arginases that have been compared to date [49], but the variation of amino acid composition shows that the *L. mexicana* enzyme is closer to the human liver arginase. The monomer structure of the arginases of both organisms and details regarding the active site showed that they are highly conserved (Fig. 3). Differences, however, can be seen between two

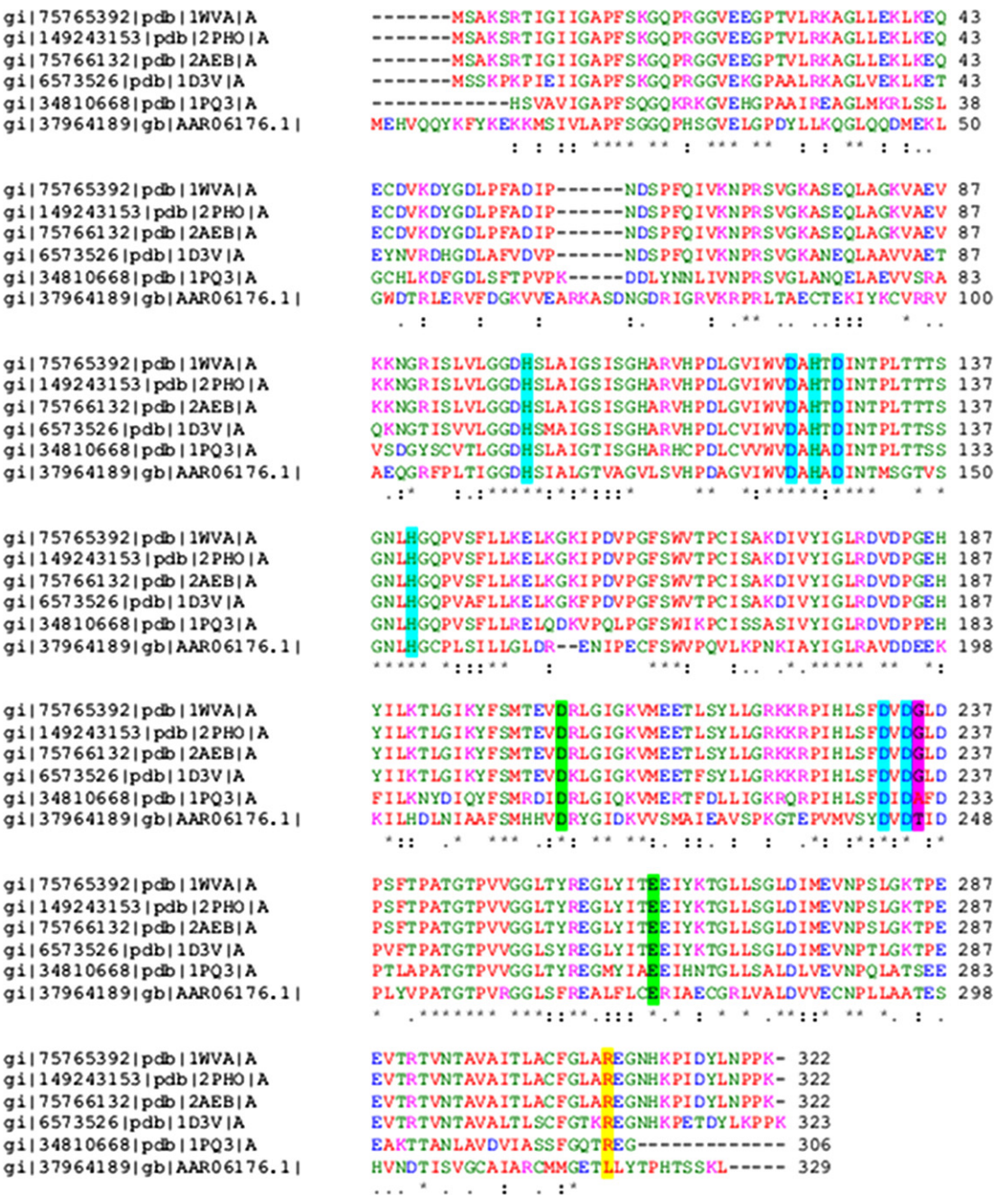

Fig. 1. Multiple sequence alignment using CLUSTALW 2.0.10. Alignment among proteins 1d3v (rat liver arginase); 1wva, 2pho, 2aeb y 1pq3 (human arginases) with the amino acid sequence of the *L. mexicana* arginase (AAR06176.1). Residues marked with blue make up the catalytic site; in the magenta is the residue that differs in the catalytic site of the *L. mexicana*; the rest of the other species, those marked in green, stabilize the trimer; in yellow is the amino acid that stabilizes the intra- and intermonomer trimer.

non-conserved equivalent amino acids, His 228 and Met 239 in the human and the *L. mexicana* arginases, respectively, forming a differential space channel-like structure (Fig. 3C). These differences in the neighborhood of the active site are not conserved and could be explored in the design of specific *L. mexicana* arginase inhibitors.

Using the crystal structure data established for the rat enzyme [48], and based on the model obtained for the monomer of the *L. mexicana* arginase, a simulation of the arginase trimer 3D structure was carried out. To our knowledge, this is the first model reported for an *L. mexicana* arginase trimer and could be useful for understanding the binding mode and for the design of new allosteric inhibitors, especially, those that bind to the interface between the monomers. This trimer model was minimized under the same conditions previously described in Section 2 (Fig. 4). The trimer model was evaluated using the same criteria as those for monomers. In the evaluation with the PROCHECK program [30], using Ramachandran plots; we observed that 80.3% of residues were located in the most favored zones and 18.9% in allowed regions. In general terms the structure has a total reliability of 99.2%. The program showed a global *G*-factor value of −0.47 obtained from the Ramachandran plot; the value must be greater than −0.5 for the model to have a good acceptance score. The QMEAN score [47] was −4.04, a low value indicates that the model is above two standard deviations. However, this may be due to the size of the protein, which is more than 900 amino acids, thus making it more difficult to measure accurately, since the QMEAN

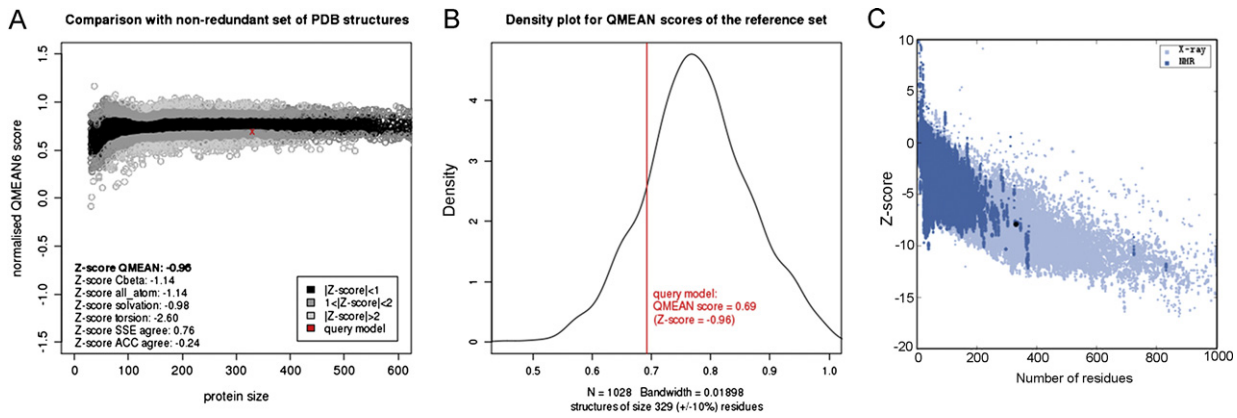

Fig. 2. QMEAN plots for the monomer of the *L. mexicana* arginase. (a) QMEAN6 plot normalized shows the standard deviation of the monomer. (b) Density plot for QMEAN. (c) Z-score plot obtained by WHATIF.

standard is up to 600 residues; over that number the graph is dispersed in measuring the standard deviation (Fig. 5).

The increase in the atomic contact score for the models for the *L. mexicana* arginase and particularly for the trimer in comparison with the monomer model suggests the existence of a trimeric structure for the *L. mexicana* arginase *in vivo*. In the rat liver arginase, the Arg308 residue forms an intramonomer salt bridge with the Glu262 and an intermonomer salt bridge with the Asp204 on the adjacent

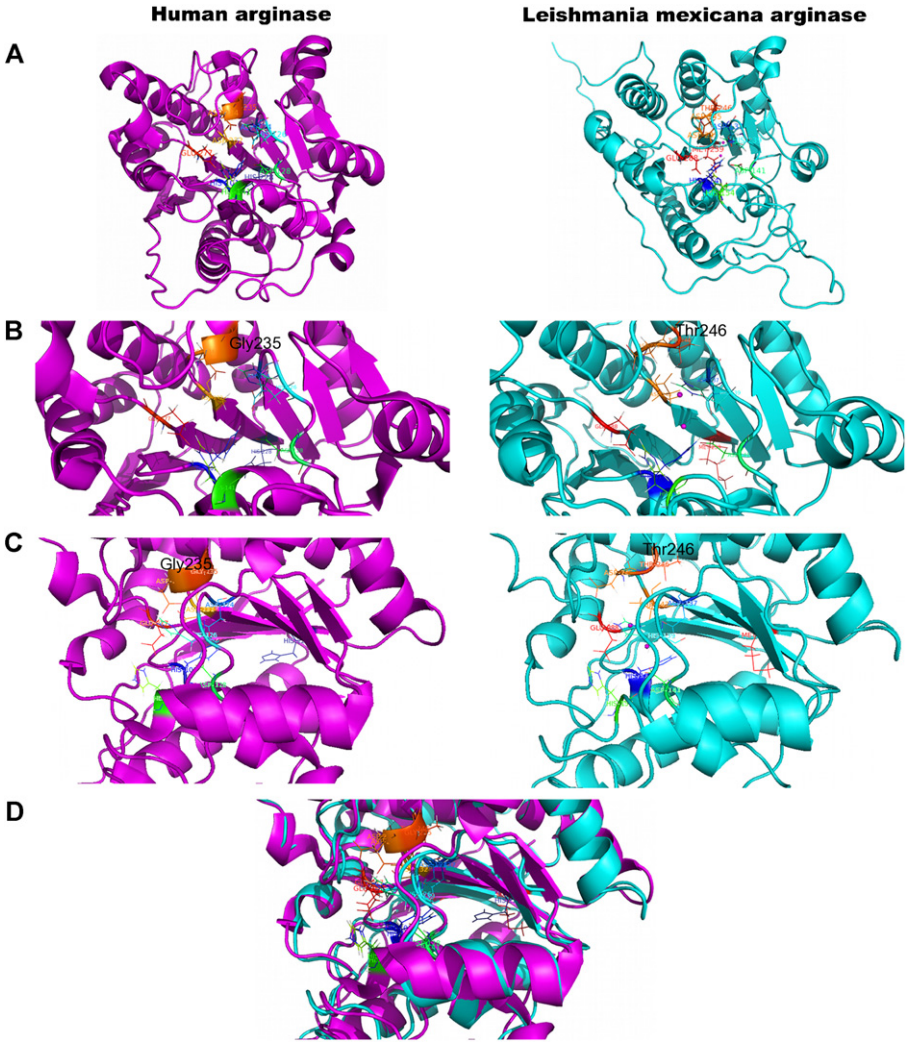

Fig. 3. *Leishmania mexicana* and the human liver type arginase 3D models. (a) The complete monomer model of both human and *L. mexicana* enzymes. Amino acids that participate in the active site are indicated by color. (b) Details of the binuclear Mn^{2+} and of the amino acids that directly interact with the substrate in the active site on both enzymes. (c) Difference in the space "channel-like" structure caused by the presence of Met239 (yellow) in *L. mexicana* instead of His228 (yellow) observed in humans. (d) Overlay of the structures of *L. mexicana* human space showing the difference in the "channel-like". Blue for the human arginase, white for the *L. mexicana* arginase.

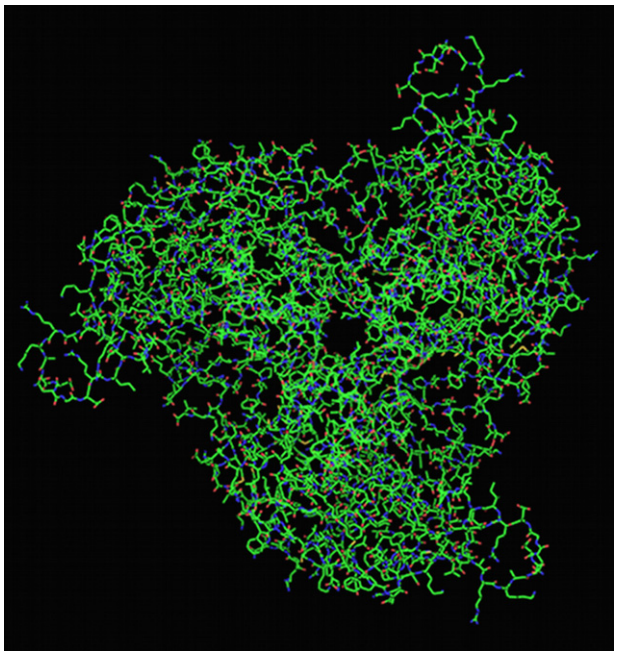

Fig. 4. Model of trimer of the *L. mexicana* arginase.

subunit [50]. Both Glu262 and Asp204 residues are conserved in the arginases of rats, humans, mice and several species of frogs of the genus *Xenopus*. These observations suggest a similar role in stabilizing the oligomeric states of the trimer. In the *L. mexicana* arginase, the Glu262 and Asp204 are conserved at positions 273 and 215, respectively, but the residue Arg308 is absent. However, in many arginases from bacteria there are hexameric arginases (dimers of trimers) rather than trimeric, and the latter three residues are not conserved. For this reason, Arg308 is not essential for the stabilization of the trimer in these organisms or for optimal activity [49].

3.2. Virtual screening

A virtual screening, using molecular docking calculations, was employed to identify molecules that could be bound to the catalytic site of the *L. mexicana* and the *H. sapiens* arginase. As described in Section 2, flexibility was allowed in all the rotable bonds of the ligand, while the protein was used as a rigid structure. Both enzymes were used in order to identify selective compounds to the catalytic site of the parasite arginase. The results of the "blind" docking showed that fewer than 100 molecules bind selectively to the catalytic site of the *L. mexicana* arginase, as depicted in Fig. 6. These molecules were submitted to a second docking, focused on the catalytic site of the arginase in order to rank them by taking into account the conformation with the lowest estimated binding energy of each compound. Based on this ranking only 18 molecules could be bound selectively to the catalytic site of the parasite with binding energies <−7.0 kcal/mol. Interestingly, 17 of the 18 compounds are analogues of the *N*-benzyl-1-alkyl-1*H*-benzimidazol-2-amines and other is a 2-ethyl-3-methyl-1-[(3-morpholin-4-ylpropyl)amino]pyrido[1,2-*a*]benzimidazole-4-carbonitrile. The structures of the 18 selective molecules and their estimated binding energies are listed in Table 3. Analyzing the structure of these compounds, it is worth noticed that most of them are 1-alkyl-2-(substituted amine)-1*H*-benzimidazole derivatives. This result shows, once again, the versatility of this structure since it presents biological activity against several parasites [37].

The protein–ligand interactions between the selected molecules and the *L. mexicana* arginase are depicted in Fig. 6. As can be observed, all molecules exhibit the same binding mode. Curiously, important interactions can be found between these molecules and the residues His114, Asp141 and His154, which directly participate in the catalytic mechanism of this enzyme. The ligand–enzyme complex is stabilized mainly by hydrogen bonds, especially those that R_2 forms with His114 and Thr257; the one between N in the 2-amine and Asp141; and some presented between N from the benzimidazole nucleus and the residue His154. Moreover, a π–π interaction can be formed between His139 and the benzyl group of the ligand. In this form, the benzyl moiety acts as an anchor toward the enzyme while benzimidazole helps to maintain the molecule in the binding pocket; the group R_1 helps to position the ligand in the catalytic site.

It is important to mention that none of these molecules has reports of measured biological activity *in vitro* against *L. mexicana* or against the *L. mexicana arginase*. The virtual screening reported in this paper shows *N*-benzyl-1-alkyl-1*H*-benzimidazol-2-amines as possible inhibitors of *L. mexicana* arginase. Even thought it is well known that the calculated binding energies do not always reflect the biological response, the specific ligand–enzyme interactions could be used as a guideline for the design of new molecules against leishmaniosis.

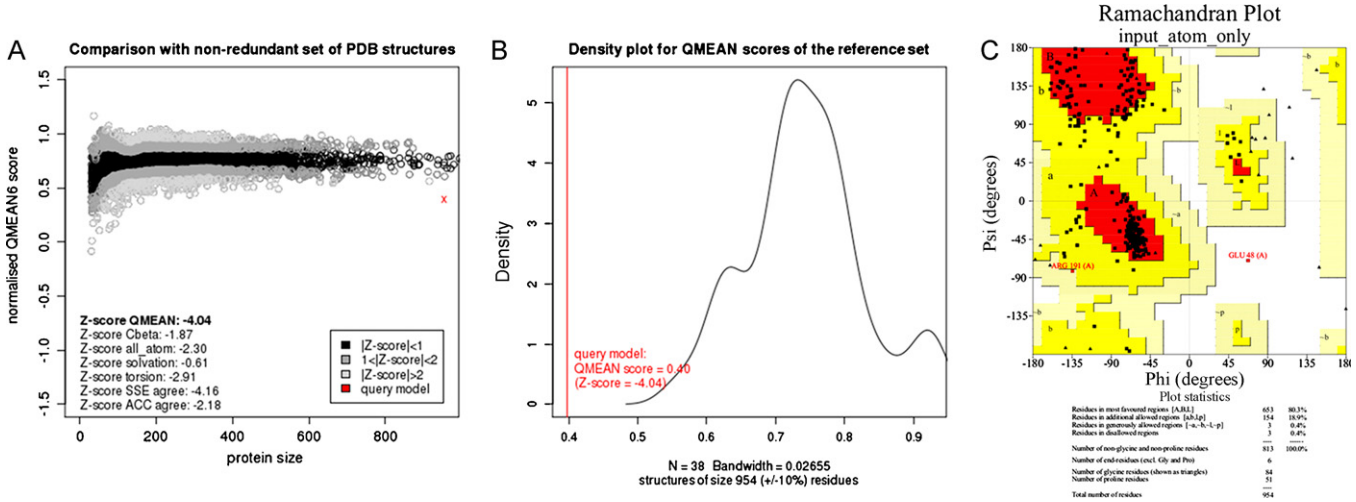

Fig. 5. QMEAN plots for the trimer of the *L. mexicana* arginase. (a) QMEAN6 plot normalized shows the standard deviation of trimer. (b) Density plot for QMEAN. (c) Ramachandran plots for the trimer that shows the most favored zones and disallowed regions.

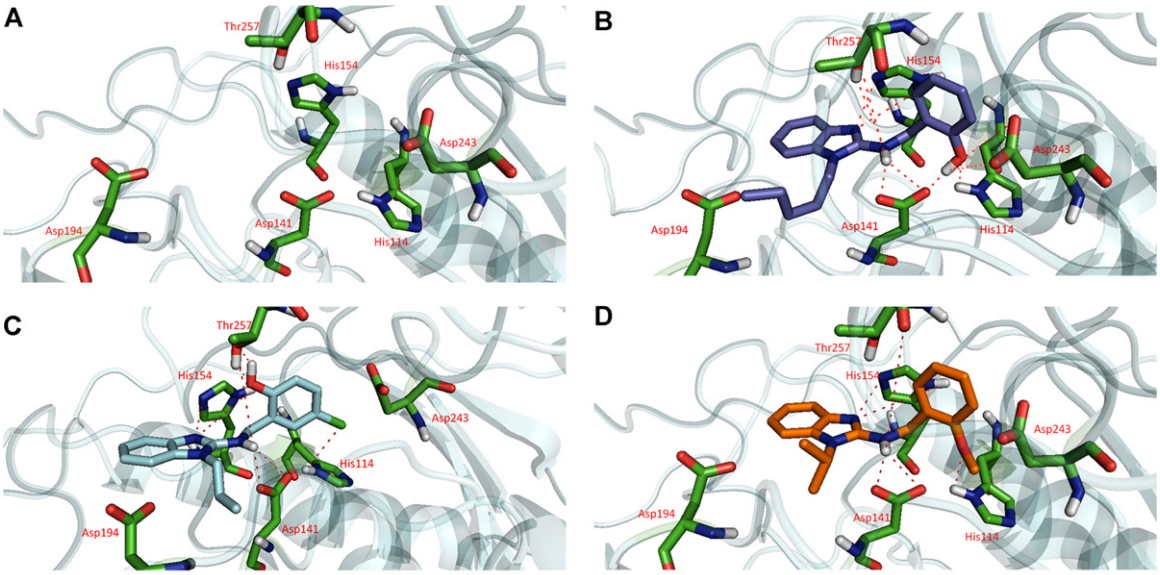

Fig. 6. Protein–ligand interactions. (A) The several ligands can interact with the protein through the amino acids His114, Asp141, His154, Thr257 and Asp243. (B) Compound 1798220 (**1**) interacts with the protein; the hydroxyl group forms a hydrogen bond with the residue His114 and Asp141; the N2 of the benzimidazole nucleus forms a hydrogen bond with the residue His154; and the N1 and N of 2-amine interact with the residue Asp141. (C) Compound 285496 (**2**) interacts with the protein; the chloro interacts with the residue His114; the hydroxyl group forms a hydrogen bond with the residue Thr257; the N2 of the benzimidazole nucleus forms a hydrogen bond with the residue His154; and the N1 and N of 2-amine interact with the residue Asp141. (D) Compound 613506 (**3**) interacts with the protein; the hydroxyl group forms a hydrogen bond with the residue His114 and Asp141; the N2 of the benzimidazole nucleus forms a hydrogen bond with the residue His154; and the N1 and N of 2-amine interact with the residue Asp141.

3.3. Molecular dynamics results

Molecular dynamics were employed to assess the stability of the homology model and of the ligand–enzyme complex. In the homology model we focused on the catalytic site, especially on the amino acids that coordinate Mn^{2+} and the interaction between the metal and the enzyme. In general, the RMSD of the Cα atoms first increased as far as a plateau at 1100 ps, indicating that equilibrium had been reached (Fig. 7A). The RMSD of the manganese through the calculation is plotted also in Fig. 7A, suggesting that the metal is stabilized in the catalytic site after 780 ps. This stabilization is caused by the relaxation of the catalytic site, in which manganeses separate

Table 3
Structure of benzimidazole derivative that binds to the *L. mexicana* arginase.

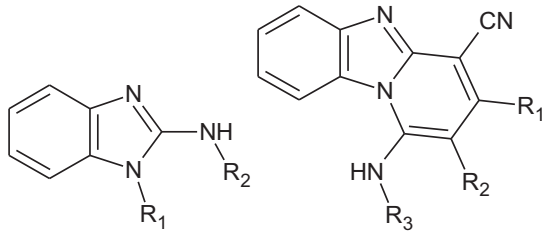

Compounds **1-17** Compound **18**

Compound	ZINC code	R_1	R_2	R_3	ΔG (kcal/mol) *L. mexicana*
1	1798220	Pentyl	2-Hydroxybenzyl		−9.1
2	285496	Propyl	5-Chloro-2-hydroxybenzyl		−8.96
3	613506	Isopropyl	2-Methoxybenzyl		−8.78
4	285488	Ethyl	2-Hydroxy-5-methylbenzyl		−8.6
5	513985	Isopentyl	Benzyl		−8.52
6	513988	Isobutyl	Benzyl		−8.4
7	111419	Methyl	5-Bromo-2-hydroxybenzyl		−8.3
8	2478054	Isopropyl	4-Bromobenzyl		−8.23
9	285495	Methyl	5-Chloro-2-hydroxybenzyl		−8.19
10	3643102	Butyl	4-Chlorobenzyl		−8.11
11	196189	Propyl	1,3-Benzodioxol-5-ylmethyl		−7.99
12	3643113	Propyl	4-Methoxybenzyl		−7.98
13	526385	Methyl	2-Methoxybenzyl		−7.96
14	2073201	Butyl	Pyridin-4-ylmethyl		−7.93
15	532233	Methyl	4-Bromobenzyl		−7.68
16	613506	Isopropyl	2-Methoxybenzyl		−7.78
17	804806	Ethyl	4-Methoxybenzyl		−7.38
18	4312478	Methyl	Ethyl	3-(Morpholin-4-yl)propyl	−8.2

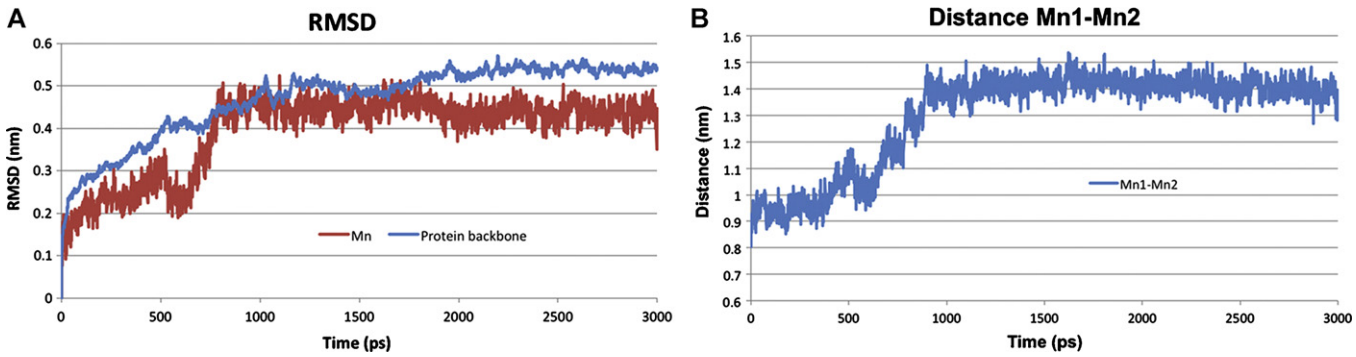

Fig. 7. (A) RMSD of the *L. mexicana* arginase monomer and RMSD of interaction with Mn^{2+} of the *L. mexicana* arginase monomer. (B) Distance between both mangeneses through all the molecular dynamics.

themselves around 1.3 nm in order to enhance the interaction with acidic residues that coordinate the metals (Fig. 7B). The residues responsible for the metal coordination are Asp 141, Asp194, Glu196 and Glu197 for Mn^{2+}–1, while Asp137, Asp243 and Glu288 coordinate Mn^{2+}–2, as shown in Fig. 8. During these calculations, it is clear that the average distance between the manganese and these acidic residues is 0.21 nm. In addition, the average distance average between the two manganeses is 1.3 nm (Fig. 7B).

As stated above, molecular dynamics simulation was used to analyze the enzyme–ligand complex and to identify the possible bioactive conformation of this molecule. For this purpose, the conformation of compound **1**, obtained from molecular docking, and the model of *L. mexicana* were used as the starting point of the simulation. The RMSD of compound **1**, plotted in Fig. 9A, shows that the ligand reaches equilibrium after 570 ps, which is faster than the protein. As discussed before, the ligand is stabilized mainly by hydrogen bonds, the ones that were analyzed throughout the molecular dynamics. The plot in Fig. 9B shows the distance between the H in the 2-amino group and the oxygen of Asp141 and Thr257. Interestingly, the formation of the hydrogen bond between the ligand and the Asp141 is stable at the beginning of the simulations (first 95 ps), but then, the amine flips to form a hydrogen bond with Thr257, at 750 ps. This result suggests that these two residues of the catalytic site can stabilize the interaction between NH and the protein; nevertheless a longer simulation is needed to support this idea.

A similar situation can be observed when analyzing the interaction between the OH of the ligand in compound **1** and Asp141 (Fig. 9C). In this case, a hydrogen bond is formed between these groups at the beginning of the calculation (60 ps). However, as the simulation moves forward (around 760 ps), the ligand is internalized and the OH is able to form a new hydrogen bond with Asp243, which is buried in the catalytic site. The interaction OH–Asp243 shows that the benzyl group moves inside of the catalytic site and that the OH interacts with several residues within the binding site (Fig. 10). It is worth mentioning that the ligand remained inside the binding site and the hydrogen bonds were constant

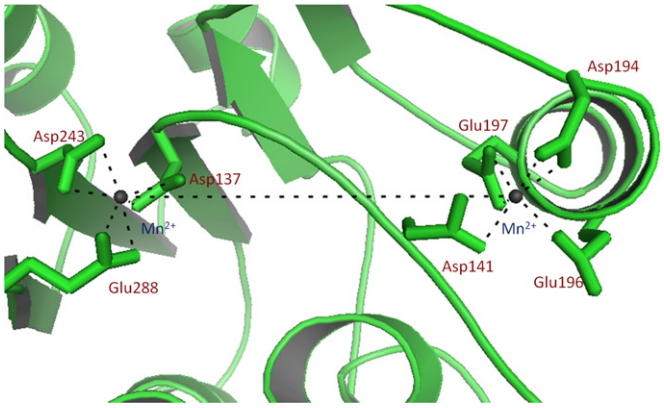

Fig. 8. Interaction between the Mn^{2+} and the residues of aminoacids. The image indicates the type of aminoacids (Glu and Asp) that stabilize the Mn and the distance between the two manganeses (an average of 1.3 nm).

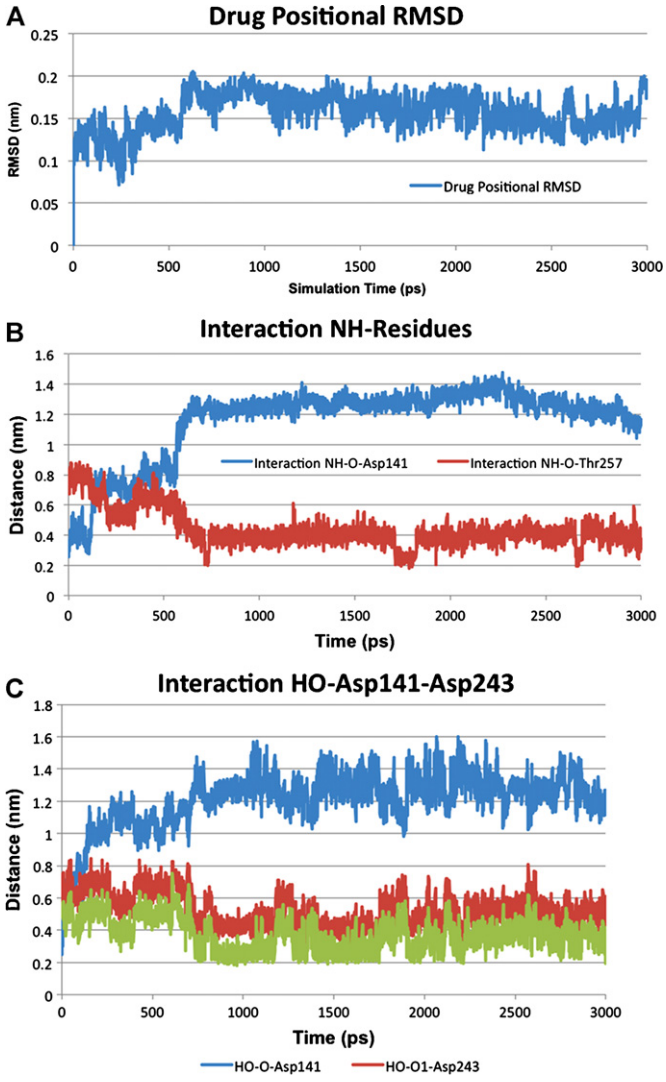

Fig. 9. (A) Drug positional RMSD. (B) Interaction of 2-Amino group with Asp141 and Thr257. (C) Interaction HO group with Asp141 and Asp243.

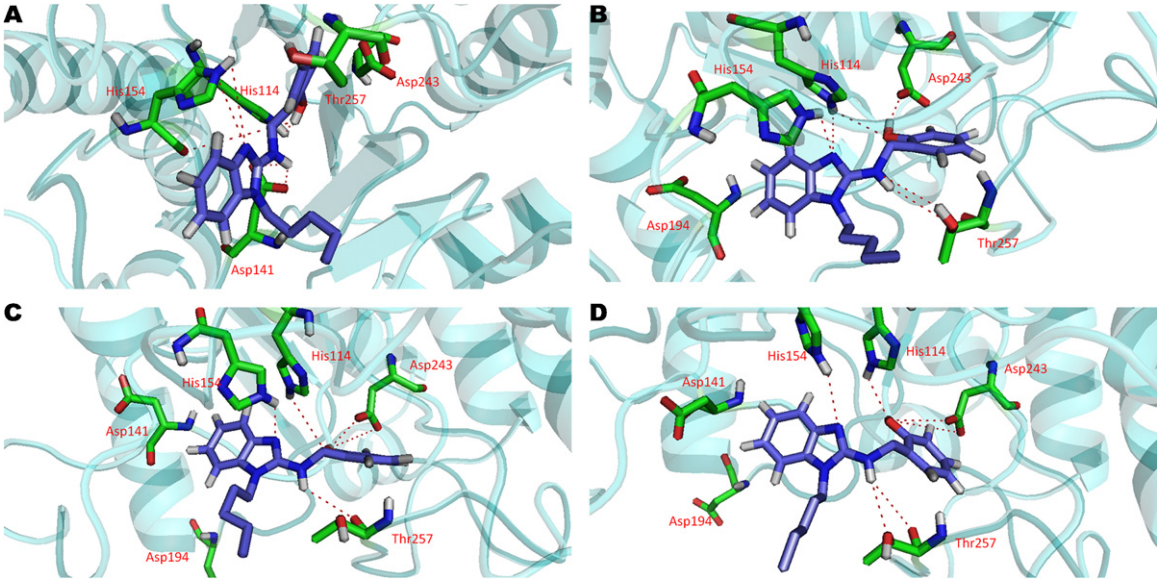

Fig. 10. Position of compound **1** inside the protein during the molecular dynamic. (A) At 1 ps time; the interaction is as shown in Fig. 6B. (B) At 1000 ps time; the initial interaction changes, thus the HO group interacts with the residue Asp243 more than His114; the NH group now changes the interaction with Thr257; the interaction of N2 of the bencimidazole nucleus is stronger than 1 ps. (C) At 2000 ps time; all the interactions in B are conserved and are stronger. (D) At 3000 ps time; the final interaction is similar to B and C.

throughout the simulation time. Furthermore, it was observed that the ligand conformation does not involved important changes. Indeed, all these results provide important information regarding the ligand–enzyme dynamical interaction (Fig. 10).

Furthermore, we have synthesized compounds **1**–**5** that were predicted to be the most active of the designed series and carried out preliminary *in vitro* evaluation on *L. mexicana* promastigotes. Results so far obtained indicate that these compounds have good activity against this stage of the parasite. However, we are still working on the synthesis of the remaining compounds (**6**–**18**) to obtain more activity data to complement this study.

4. Conclusions

Although several three-dimensional structures with homologous sequences to the *L. mexicana* arginase were found using three different search methods (GenSilico, PDB/BLAST, and Bioinfobank), only the crystal structures of the *H. sapiens* arginase (PDB ID: 2aeb [43]) and *R. norvergicus* (PDB ID: 1d3v [44]) had a high percentage of similarity (above 40%) with the parasite enzyme. This information, coupled with the reported amino acids in the catalytic site of the three arginases, which differ in one amino acid, suggests that specific inhibitors could be designed for the *L. mexicana* arginase. On the other hand, the best model for the three-dimensional structure of the *L. mexicana* arginase was obtained using the *R. norvergicus* crystal structure. The best model of the *L. mexicana* arginase was used to perform a virtual screening with 1439 benzimidazole derivatives. Among these molecules, *N*-benzyl-1-alkyl-1*H*-benzimidazol-2-amines were identified as possible selective inhibitors of the *L. mexicana* arginase. The molecular dynamics simulations revealed the stability of the monomer of arginase as well as the stability of the ligand–protein complex. The results further suggest that His114, Asp141, Asp194 Asp243 and Thr257 could play an important role for the further optimization of selective inhibitors.

Acknowledgements

Méndez-Cuesta CA is very grateful to Consejo Nacional de Ciencia y Tecnología (CONACyT) for granting scholarship 170430/170430. We acknowledge DGSCA, UNAM for the support we received to use the HP Cluster Platform 4000 Opteron dual core supercomputer (KanBalam).

References

[1] M. Ouellette, Biochemical and molecular mechanisms of drug resistance in parasites, Tropical Medicine and International Health 6 (2001) 874–882.
[2] A. Armson, S.W. Kamau, F. Grimm, J.A. Reynoldson, W.M. Best, L.M. MacDonald, R.C.A. Thompson, A comparison of the effects of a benzimidazole and the dinitroanilines against *Leishmania infantum*, Acta Tropica 733 (1999) 303–311.
[3] S. Khabnadideh, D. Pez, A. Musso, R. Brun, L.M. Ruiz Pérez, D. González-Pacanowska, I.H. Gilbert, 2,4-Diaminopyrimidines as inhibitors of leishmanial and trypanosomal dihydrofolate reductase, Bioorganic and Medicinal Chemistry 11 (2003) 4693–4711.
[4] Organización Mundial de la Salud, Lucha contra las leishmaniasis. Serie de Informes Técnicos No. 793, OMS, Ginebra, 1990.
[5] López de Cogolludo D, Historia de Yucatán, Mérida. Edición original, Madrid, 1688, Reeditado por la Universidad de Yucatán, 1978.
[6] F. Biagi, Síntesis de 70 historias clínicas de leishmaniasis tegumentaria de México (úlcera de los chicleros), Rev Facultad de Medicina UNAM 33 (1953) 385–396.
[7] N.F. Andrade, M.M. García, R.A. Cruz, L.S. Canto, D.E. Simmonds, Estudio preliminar de correlación clínica, histológica e inmunológica de la leishmaniasis cutánea mexicana en el hombre, Archivos de Investigación Médica (México) 15 (1984) 267–280.
[8] C.O. Velasco, S.J. Savarino, B.C. Walton, A.A. Gamm, F.A. Neva, Diffuse cutaneous leishmaniasis in Mexico, American Journal of Tropical Medicine and Hygiene 41 (1989) 280–288.
[9] Tellaeche M, Informe relativo a prevención y control de las leishmaniasis en México, in: Dirección de Prevención y Control de Enfermedades Transmitidas por Vectores, Secretaría de Salud, México, 1993.
[10] D. Sereno, A. Cordeiro da Silva, F. Mathieu-Daude, A. Ouaissi, Advances and perspectives in leishmania cell based drug-screening procedures, Parasitology International 56 (2007) 3–7.
[11] D.O. Santos, C.E. Coutinho, M.F. Madeira, C.G. Bottino, R.T. Vieira, S.B. Nascimento, A. Bernardino, S.C. Bourguignon, S. Corte-Real, R.T. Pinho, C.R. Rodrigues, H.C. Castro, Leishmaniasis treatment – a challenge that remains: a review, Parasitology Research 103 (1) (2008) 1–10.
[12] UNICEF-UNDP-WHO Reports of TDR (Tropical Diseases Research). http://www.who.int/tdr/diseases-topics/leishmaniasis/en/index.html, 2011 (accessed 13.02.12).
[13] C.G. Havens, N. Bryant, L. Asher, L. Lamoreaux, S. Perfetto, J.J. Brendle, K.A. Werbovetz, Cellular effects of leishmanial tubulin inhibitors on *L. donovani*, Molecular and Biochemical Parasitology 110 (2000) 223–236.
[14] Reports of the World Health Organization. www.who.int/leishmaniasis/burden/en/, 2011 (accessed 13.02.12).
[15] S.L. Croft, G.H. Coombs, Leishmaniasis – current chemotherapy and recent advances in the search for novel drugs, Trends in Parasitology 19 (11) (2003) 503–508.

[16] M.W. Nowicki, Design, synthesis and trypanocidal activity of lead compounds based on inhibitors of parasite glycolysis, Bioorganic & Medicinal Chemistry 16 (9) (2008) 5050–5061.
[17] C. Doerig, L. Meijer, J.C. Mottram, Protein kinases as drug targets in parasitic protozoa, Trends in Parasitology 18 (8) (2002) 366–371.
[18] D.J. Rigden, S.E. Phillips, P.A. Michels, L.A. Fothergill-Gilmore, The structure of pyruvate kinase from *Leishmania mexicana* reveals details of the allosteric transition and unusual effector specificity, Journal of Molecular Biology 291 (1999) 615–635.
[19] E. Da Silva, T. Castilho, F. Pioker, C. Tomich de Paula, L. Floeter-Winter, Genomic organization and transcription characterization of the gene encoding *Leishmania amazonensis* arginase and its protein structure prediction, International Journal for Parasitology 32 (2002) 727–737.
[20] E.R. da Silva, M.F. Laranjeira da Silva, H. Fischer, R.A. Mortara, M.G. Mayer, K. Framesqui, A.M. Silber, L.M. Floeter-Winter, Biochemical and biophysical properties of a highly active recombinant arginase from *Leishmania* (*Leishmania*) *amazonensis* and subcellular localization of native enzyme, Molecular and Biochemical Parasitology 159 (2) (2008) 104–111.
[21] S.C. Roberts, M.J. Tancer, M.R. Polinsky, K.M. Gibson, O. Heby, B. Ullman, Arginase plays a pivotal role in polyamine precursor metabolism in Leishmania. Characterization of gene deletion mutants, Journal of Biological Chemistry 279 (22) (2004) 23668–23678.
[22] M.A. Kurowski, J.M. Bujnicki, GeneSilico protein structure prediction meta-server, Nucleic Acids Research 31 (2003) 3305–3307.
[23] S.F. Altschul, T.L. Madden, A.A. Schäffer, J. Zhang, Z. Zhang, W. Miller, D.J. Lipman, Gapped BLAST and PSI-BLAST: a new generation of protein database search programs, Nucleic Acids Research 25 (1997) 3389–3402.
[24] K. Ginalski, A. Elofsson, D. Fischer, L. Rychlewski, 3D-Jury: a simple approach to improve protein structure predictions, Bioinformatics 19 (8) (2003) 1015–1018.
[25] R. Chenna, H. Sugawara, T. Koike, R. Lopez, T.J. Gibson, D. Higgins, J. Thompson, Multiple sequence alignment with the clustal series of programs, Nucleic Acids Research 31 (13) (2003) 3497–3500.
[26] P.A. Bates, L.A. Kelley, R.M. MacCallum, M.J.E. Sternberg, Enhancement of Protein modelling by human intervention in applying the automatic programs 3D-JIGSAW and 3D-PSSM, Proteins: Structure, Function and Genetics (Suppl. 5) (2001) 39–46.
[27] B. Contreras-Moreira, P.A. Bates, Domain Fishing: a first step in protein comparative modelling, Bioinformatics 18 (2002) 1141–1142.
[28] A. Sali, T.L. Blundell, Comparative protein modelling by satisfaction of spatial restraints, Journal of Molecular Biology 234 (1993) 779–815.
[29] A. Fiser, R.K. Do, A. Sali, Modeling of loops in protein structures, Protein Science 9 (2000) 1753–1773.
[30] R.A. Laskowski, M.W. MacArthur, D.S. Moss, J.M. Thornton, PROCHECK: a program to check the stereochemical quality of protein structures, Journal of Applied Crystallography 26 (1993) 283–291.
[31] R.W. Hooft, G. Vriend, C. Sander, E.E. Abola, Errors in protein structures, Nature 381 (1996), p. 272.
[32] E.G. Hutchinson, J.M. Thornton, PROMOTIF: a program to identify and analyze structural motifs in proteins, Protein Science 5 (2) (1996) 212–220.
[33] K. Arnold, L. Bordoli, J. Kopp, T. Schwede, The SWISS-MODEL workspace: a web-based environment for protein structure homology modelling, Bioinformatics 22 (2006) 195–201.
[34] W.L. DeLano, The PyMOL Molecular Graphics System, DeLano Scientific LLC, Palo Alto, CA, 2007, http://www.pymol.org
[35] SYBYL Software Package, Version 8.0, Tripos Associates Inc., S. Hanley Rd., St. Louis, MO 631444, USA, 1699.
[36] J.J. Irwin, B.K. Shoichet, ZINC – a free database of commercially available compounds for virtual screening, Journal of Chemical Information and Modeling 45 (1) (2005) 177–182.
[37] J. Valdez, R. Cedillo, A. Hernández-Campos, L. Yépez, F. Hernández-Luis, G. Navarrete-Vázquez, A. Tapia, R. Cortés, M. Hernández, R. Castillo, Synthesis and antiparasitic activity of 1*H*-benzimidazole derivatives, Bioorganic & Medicinal Chemistry Letters 12 16 (19) (2002) 2221–2224.
[38] S. Díaz, M. de los Remedios, Síntesis de derivados del 1-metilbencimidazol con actividad antihelmíntica potencial, Master of Science Dissertation, Universidad Nacional Autónoma de México, 1999.
[39] Méndez-Cuesta, Carlos Alberto, Síntesis y actividad antiparasitaria del 6-Cloro-2-(metiltio)-N-(5-nitro-1,3-tiazol-2-il)-1H-bencimidazol-5-carboxamida y sus derivados 1-metilados. Medicinal Chemistry Dissertation, Universidad Nacional Autónoma de México, 2005.
[40] F. Hernández-Luis, A. Hernández-Campos, R. Castillo, G. Navarrete-Vázquez, O. Soria-Arteche, M. Hernández-Hernández, L. Yépez-Mulia, Synthesis and biological activity of 2-(trifluoromethyl)-1*H*-benzimidazole derivatives against some protozoa and *Trichinella spiralis*, European Journal of Medicinal Chemistry 45 (7) (2010) 3135–3141.
[41] M.F. Sanner, Python: a programming language for software integration and development, Journal of Molecular Graphics and Modelling 17 (1999) 57–61.
[42] A.W. Schuttelkopf, D.M.F. Van Aalten, PRODRG – a tool for high-throughput crystallography of protein–ligand complexes, Acta Crystallographica 60 (2004) 1355–1363.
[43] L. Di Costanzo, G. Sabio, A. Mora, P.C. Rodriguez, A.C. Ochoa, F. Centeno, D.W. Christianson, Crystal structure of human arginase I at 1.29-A resolution and exploration of inhibition in the immune response, Proceedings of the National Academy of Sciences USA 102 (2005) 13058–13063.
[44] J.D. Cox, N.N. Kim, A.M. Traish, D.W. Christianson, Arginase–boronic acid complex highlights a physiological role in erectile function, Natural Structural Biology 6 (1999) 1043–1047.
[45] L. Di Costanzo, M.E. Pique, D.W. Christianson, Crystal structure of human arginase I complexed with thiosemicarbazide reveals an unusual thiocarbonyl μ-sulfide ligand in the binuclear manganese cluster, Journal of the American Chemical Society 129 (2007) 6388–6389.
[46] E. Cama, D.M. Colleluori, F.A. Emig, H. Shin, S.W. Kim, N.N. Kim, A.M. Traish, D.E. Ash, D.W. Christianson, Human arginase. II. Crystal structure and physiological role in male and female sexual arousal, Biochemistry 42 (2003) 8445–8451.
[47] P. Benkert, M. Biasini, T. Schwede, Toward the estimation of the absolute quality of individual protein structure models, Bioinformatics 27 (3) (2011) 343–350.
[48] Z.F. Kanyo, L.R. Scolnick, D.E. Ash, D.W. Christianson, Structure of a unique binuclear manganese cluster in arginase, Nature 383 (1996) 554–557.
[49] J. Perozich, J. Hempel, MorrisF S.M. Jr., Roles of conserved residues in the arginase family, Biochimica et Biophysica Acta 1382 (1998) 23–37.
[50] L.T. Lavulo, T.M. Sossong Jr., M.R.B. Burke, M.L. Doyle, J.D. Cox, D.W. Christianson, D.E. Ash, Subunit–subunit interactions in trimeric arginase, Journal of Biological Chemistry 276 (2001) 14242–14248.